Material and Methods:

Chemicals: All the chemicals unless specified were purchased from Sigma-Aldrich. Immunohistological staining materials were purchased from Molecular Probes (Life Technologies). Goat Anti-Rabbit IgG-DyLight 680 was obtained from Thermo Scientific and mounting media DAPI or TRITC-Phalloidin from Vector Laboratories. The screen-well ion channel ligand library was acquired from Enzo Lifesciences. Microscint light scintillation cocktail was purchased from Perkin Elmer.

Isotope production and quality control: [^{223}Ra]$RaCl_2$ was produced as previously described method (*1*), pure ^{223}Ra was generated from the parent isotope ^{227}Th or ^{227}Ac source provided by Oak Ridge, Department of Energy. Briefly, 10-20 µCi of the parent isotope was adsorbed on an anionic polymeric resin Dowex 1x8 and eluted under mild acidic conditions (methanol: nitric acid (2N) 80:20) to isolate pure ^{223}Ra-nitrates. Following multiple evaporations in metal free water, the final sample was suspended in sodium citrate (0.03 M) and saline (150 mM). The radiochemical quality was checked using gamma spectrometry with a High Purity Germanium detector, showing undetectable isotopic parent breakthrough and a ^{223}Ra radiochemical purity of over 99%.

In vitro studies: To establish intestinal cellular models, we cultured human duodenal enteroids and Caco-2/BBe1 monolayers on Transwell polymeric filter plates divided into lower and upper incubation compartments, modeling the basolateral and apical side of the epithelium, respectively. This setup permitted the identification and quantification of ^{223}Ra transcellular transport, mimicking the physiological exsorption of ^{223}Ra.

Human duodenal enteroids from healthy patient-derived cellular crypts tissue samples were reconstituted and grown. Both differentiated (DF) and undifferentiated (UDF) phenotypes were tested. DF monolayers were induced by removal of Wnt3A and Rspondin-1 DFM factors from the incubation media, as described (*2*). DF cell state corresponds to villus-like cells, with higher cell heights, increased TEER and larger microvilli density as compared to UDF related to crypt-like cells. DF enteroids present higher density of NHE3 ion transporters (26% higher than UDF) and lower density of NKCC1 transport (89% less than UDF)(*3*,*4*).

DF or UDF duodenal enteroids were seeded and grown inverted (villi upward) on 6-transwell plates for 2 weeks until cell confluence was reached, leading to confluent monolayers. Monolayer integrity was checked, before and after [^{223}Ra]$RaCl_2$ incubation, by measuring surface tension TEER in Ω/m (transepithelial electrical resistance) utilizing an ohmmeter. 50 nCi (1.85 kBq) was added in the basolateral compartment and incubated at 37 °C, 5% CO_2, 1 to 24 h (n=4) before separating well for analyses. Radioactive transport was measured utilizing light scintillation counting (Topcount, PerkinElmer). Radium-223 passage was calculated as the ratio percentile of the apical sampling counts per minute (cpm) over the initial activity added; including background correction.

Caco-2/BBe1 (brush border expressing clone) monolayers were utilized for ion-channel ligand library screening (52 compounds – see Suppl. Info.) testing radioactive transfer upon epithelial ion-transport activation or blocking. Caco-2/BBe1 cells were seeded 15,000 cells per well in 96-well transwell filter plates and assayed 10 days post-seeding. The screened bioactive material was added in the basolateral well (20 µM, n=3 / molecules). 2 h following drug incubation, 3

nCi (0.1 kBq) of [^{223}Ra]$RaCl_2$ was added in the same compartment. The incubation was stopped 4 h post ^{223}Ra addition to assess radioactive transfer from basolateral to apical compartments.

The monolayer integrity was verified using lucifer yellow permeability assay. The fluorescent tracer was added in the apical compartment post-incubation, and fluorescence permeability was read sampling the basolateral media. The percent of Lucifer Yellow Passage (LYp%) was calculated as the ratio of relative Fluorescence Units-535 nm (FU) of the assayed basolateral sample over FU of a control complete transfer to the basolateral compartment (ruptured membrane). Any monolayers presenting LYp% > 1.5 were excluded from the experiment, deemed to have been damaged.

Radioactive reading was accomplished sampling the apical compartments on Luma plates and reading the dried luminescence using Topcount scintillation counter. A control assay modulator-free receiving only [^{223}Ra]$RaCl_2$, #12: control, was carried out defining the natural radioactive flux (^{223}Ra passage %) occurring through cells as the baseline value 0. Averaged (n=3) drug-assayed measurements were normalized to modulator-free flux. Results were plotted as a waterfall chart: with negative values showing ^{223}Ra blocking and positive values showing ^{223}Ra transport activation through monolayers.

List of 52 evaluated compounds in the Caco-2 monolayer screening (Figure 2)

The compounds evaluated were selected from the ion channel library (Screenwell, Enzo). 1: Fipronil: GABA-gated chloride-channel blocker; 2: Amiloride HCl.2H_2O: NaH channel blocker; 3: Bezamil.HCl: NaH Channel blocker; 4: AM92016: K^+ channel blocker; 5: SDZ-201 106(+/-) Na^+ channel indirect activator and K channel blocker; 6: N-phenylanthranilic acid, Cl^- channel blocker; 7: Tetrandrine: Ca^{2+} channel blocker; 8:TMB-8HCl intracellular Ca^{2+}-channel antagonist; 9: Dantrolene: Ca^{2+} channel blocker; 10 Niguldipine.HCl: Ca^{2+} channel blocker; 11: Thapsigargin: Ca^{2+} -ATPase inhibitor; 12: control saline untreated well; 13: FPL-64176: Ca^{2+} channel blocker; 14: Niflumic acid: Cl^- channel inhibitor; 15: SKF-96365: cation channel inhibitor; 16: Nitrendipine: Ca^{2+} channel blocker; 17 Procainamide.HCl: voltage-gated Na channel blocker; 18: E-4031.2HCl.2H2O: K^+ channel blocker of the hERG-type; ZM226600: K^+/ATP channel activator; 20: Aconitine: Na^+ channel activator; 21: Penitrem A: K^+-channel inhibitor; 22: Nicardipine: Ca^{2+} channel blocker; 23: PCO-400: K^+ channel activator; 24: Quinine HCl.2H_2O Ca^{2+}-activated K^+ channel blocker; 25: Amiodarone: K^+ channel inhibitor; 26: Amlodipine Ca^{2+} channel blocker; 27: Pimozide K^+ channel inhibitor; 28: 2',4'-Dichlorobenzamil.HCl: Na^+/ Ca^{2+} channel modulator; 29: Diazoxide: K^+ channel activator; 30: Verapamil. HCl: Ca^{2+} channel blocker; 31: Cyclopiazonic acid: Ca^{2+} channel modulator; 32: Gingerol: ion channel activator; Veratridine Na^+ channel activator; 34: Fluspirilene: Ca^{2+} channel blocker; 35: R-(+)IAA-94 Cl channel modulator; 36: Lidocaine.HCl.H_2O: Na^+ channel blocker; 37: Nifedipine Ca^{2+} channel blocker; 38: U-37883A ion channel blocker; 39: Flufenamic acid: ion channel modulator; 40: Phetolamine HCl: K^+/ATP channel blocker; 41: Ryanodine: intracellular Ca^{2+} channel modulator; 42: Paxilline: K^+ channel blocker; 43: 5-Hydroxydecanoic acid: Na^+/K^+ channel opener; 44: Numodipine K^+ channel blocker; 48: Propafenone: K^+ channel blocker; 49: QX-314 bromide: Na^+ channel blocker; 50: Flecainide acetate Na^+ channel blocker; 51: NS-1619: BKCa channel opener; 52: Flunarizine.2HCl: Ca^{2+} -antagonist; 53: Quinidine. HCl H2O Na^+channel blocker

In vivo studies: All animal experiments were conducted in accordance with the institutional animal care and use protocol of both the Johns Hopkins University School of Medicine and Washington University School of Medicine as well as conformed to the Guide for the Care and Use of Laboratory Animal (8^{th} Ed. National Research Council of the National Academies).

Immunohistological staining: Male C57Bl/6 mice aged 20-30 weeks old were intravenously administered with 250 kBq/kg of [^{223}Ra]$RaCl_2$. Animals were fed with Golytely (24g/350 mL) 2 h prior to injection. The study was terminated 24 h post treatment. Portions of each GI region (1 cm) duodenum, jejunum, ileum and colon were promptly harvested. GI specimens were coated with OCT and flash frozen. Transversal sectioning of GI tissues was conducted utilizing Leica 1860 microtome at 10 µm thickness. GI tissue sections were fixed by immersion in 10% paraformaldehyde (PFA) for 15 min followed by washing with Phosphate Buffered Saline 1x. Following fixation, tissues were directly mounted on slides using DAPI and/or TRITC-Phalloidin media under cover slip and imaged on a Zeiss Axioplan M1 using µmanager (version 2.0)(*6*).

For TUNEL staining, tissues were permeabilized, treated with 0.25% Triton x-100 for 15 min and washed with PBS. A second fixation using 10% PFA was performed, with slides washed with deionized water. Tissues were then subjected to buffer reaction mixtures from the Click-iT Plus TUNEL assay. Positive controls were included, with an additional DNAase treatment. Final counterstaining used Hoechst33342 (1:5000) before mounting tissue specimen under cover slip with 30% aqueous glycerol.

For γH2AX staining, tissues were fixed and underwent blocking using serum reagent, 1 h at room temperature. The primary antibody (γH2AX, rabbit antibody 1mg/mL– 1:50) was applied overnight at 4 °C in humidity chamber. Tissues were then washed and prepared for secondary antibody development using goat anti-rabbit IgG Alexa Fluor 488 (1:200) 1 h at 4 °C in humidity chamber. The resulting samples were washed, counterstained using Hoechst 3342 and mounted under cover slip with glycerol 30%.

Kidneys were collected 20 days post-treatment and the tissues were fixed in formalin for 72 h then transferred to 70% ethanol. Tissues were processed by dehydration, paraffin embedding, and sectioning at 4 µm. Adjacent sections were stained with H&E, PAS and Masson's trichrome.

Response experiments and imaging

Dosimetry: Mean absorbed radiation doses were estimated using the source and target organ framework outlined by the MIRD Committee (*7*). The mean activity of each organ at each time point (from 15 min to 10 days p.i.; Fig 3E) was used for calculations. The cumulated activity in each organ was calculated using the trapezoidal rule over the 10 days measurement. This information was entered into the program RODES (*8*,*9*). This program includes a set of anatomical mouse models. RODES computes the absorbed dose of each organ using SAF calculated for various energies of alpha particles, photons and electrons by Monte Carlo simulation using MCNPX 2.6.

Osteosarcoma murine model: Male R2G2 mice >12 wks of age (Envigo) were inoculated with 5 million SAOS2 cells in the flank and tumors grown for 100 days until mineral protuberances were detected by X-ray (Faxitron MX20). Mice were separated in 2 cohorts (n=3). We compared ^{223}Ra organ distribution with, and without, amiloride-combination treatment at 24 h post-injection. Kidney, cecum, femurs and osteosarcoma tumor tissues were collected and evaluated for gamma counting and tissue weighing %IA/g. *In vivo* whole body and post-mortem bones and osteosarcoma were imaged using x-ray to confirm the mineralization of the tumor.

Intratibial C4-2B tumor growth inhibition: 12 skeletally mature male R2G2 mice (>12 weeks old, Envigo) received intratibial inoculation of luciferase transduced C4-2B human prostate cancer cell line (*10*). 0.25 million cells were implanted in the tibia shaft. Bone tumor growths were monitored over 55 days using bioluminescent imaging with the IVIS Lumina small animal scanner (PerkinElmer). Intravenous administration of luciferin (1:1 in saline) 50 μL was conducted 2 min prior to optical imaging. Images were processed utilizing Living Image Version 4.2 software.
For treatment administration, animals were randomized in 3 cohorts (n=4), cohort (1) [^{223}Ra]$RaCl_2$; (2) [^{223}Ra]$RaCl_2$ + Amiloride; (3) Amiloride. Each group received treatments 20 days post tumor inoculation. Animals received the diuretic Amiloride dosed 12.5 mg/kg i.p. (for cohort 2 & 3) 1 h prior to [^{223}Ra]$RaCl_2$ dosed 7.4 kBq / 100 μL i.v. for cohort 1 & 2. Tumor bearing legs were monitored via bioluminescent acquisitions twice a week recording radiance normalized to values of day 0 treatment. Mice weights were recorded over the course of the experiment. The experiment was terminated 55 days post inoculation following X-rays acquisition of the disease site.

Toxicity evaluation: Healthy male mice FVB/NCR aged 14 weeks (n=5) were randomized into 4 cohorts treated with 1) [^{223}Ra]$RaCl_2$ alone (3.7 KBq/100 μL); or 2) amiloride alone (12.5 mg/kg i.p.); or 3) combination amiloride with [^{223}Ra]$RaCl_2$ or 4) control untreated (saline). The animals were maintained for 20 days following treatment with food and water and submitted to blood chemistry analysis (Abaxis Vscan 2) at day 1; 7 and 19 days. Weight was monitored for each cohort over 20 days. At the end of the study (day 20 post-treatment), animals were sacrificed and whole limbs and kidneys were harvested for gamma counting and histopathological assessments.

Dose and schedule for amiloride combination treatment: Ion channel modulators are characterized with transient activity profiled, with efficacy waning approximately 1-2 h post administration (*11*,*12*). Administered doses of the inhibitor (13 mg/kg; 26 mg/kg) and different times of amiloride administration (15 min, 1 h, 3 h) prior to [^{223}Ra]$RaCl_2$ were tested to comparatively evaluate ^{223}Ra distribution. Organs were harvested at 24 h following [^{223}Ra]$RaCl_2$ administration. The organs distribution data are shown in Supplemental Figure 3 and 4. No significant differences were found in organ distribution whether changing doses or time of amiloride injections relative to [^{223}Ra]$RaCl_2$. For all other amiloride combination studies, 12.5-13mg/kg amiloride dosage and i.p. injection 1 h prior [^{223}Ra]$RaCl_2$ were the chosen parameters.

Statistics: All P-values were calculated with unpaired two-tailed t-test with equal Standard Deviation (SD), utilizing Graphpad, Prism software (version 6D). Significant differences were expressed at $P<0.05$ and $P<0.1$ for *in vitro* (n>4) and *in vivo* experiments (n>6).

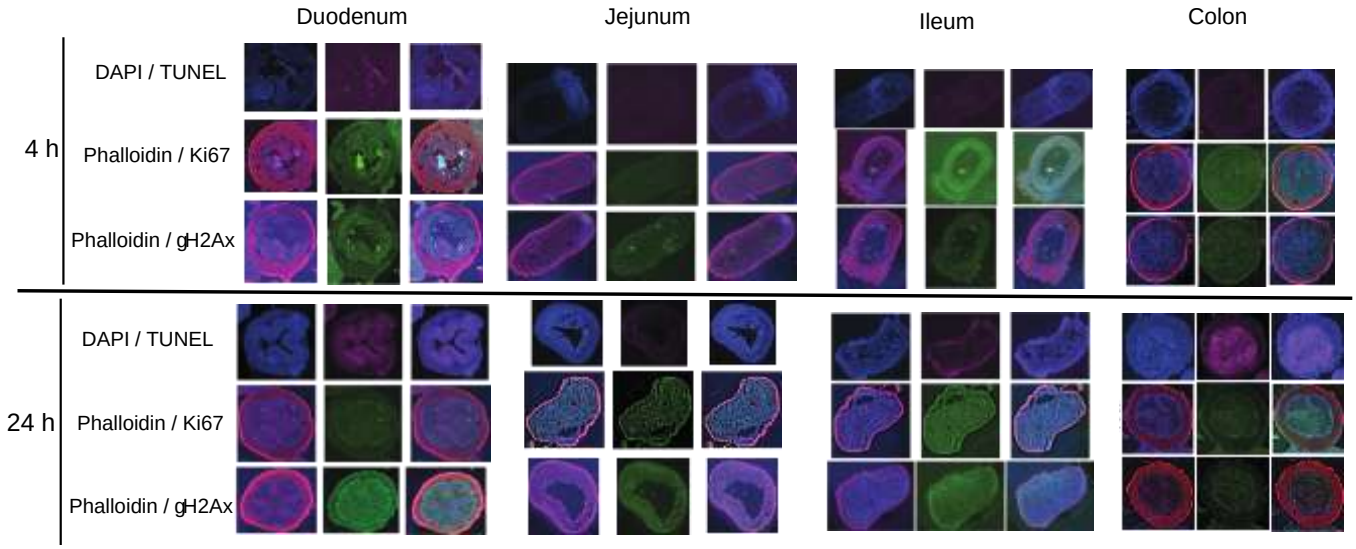

Supplemental Figure 1: Immunofluorescence by DAPI, TUNEL, Ki67 and γH_2AX of duodenum, jejunum, ileum and colon tissue sections following [^{223}Ra]$RaCl_2$ administration. Tissues were harvested at 4 (upper panels) and 24 h (lower panels) post-^{223}Ra injection.

For each organ panel, the first line displays DAPI and TUNEL staining: with upper left corner DAPI in blue displaying cell nuclei and middle slide presenting TUNEL in purple and overlaid with DAPI in the right; the second line shows Phalloidin and Ki67: middle left displays phalloidin (red + blue) staining cytoskeletal structures; middle and right corner slides present Ki67, marker of cell proliferation, in green and overlaid with phalloidin in the right; the third line shows Phalloidin and γH_2AX: phalloidin (red + blue in the left corner), the lower middle slide presents γH_2AX (green) recognizing DNA damage and overlay with phalloidin (far rights). Of all organs and time points, only duodenum and colon at 24 h post-^{223}Ra administration presented both γ-H2AX and TUNEL positive staining following ^{223}Ra alpha emission related damages.

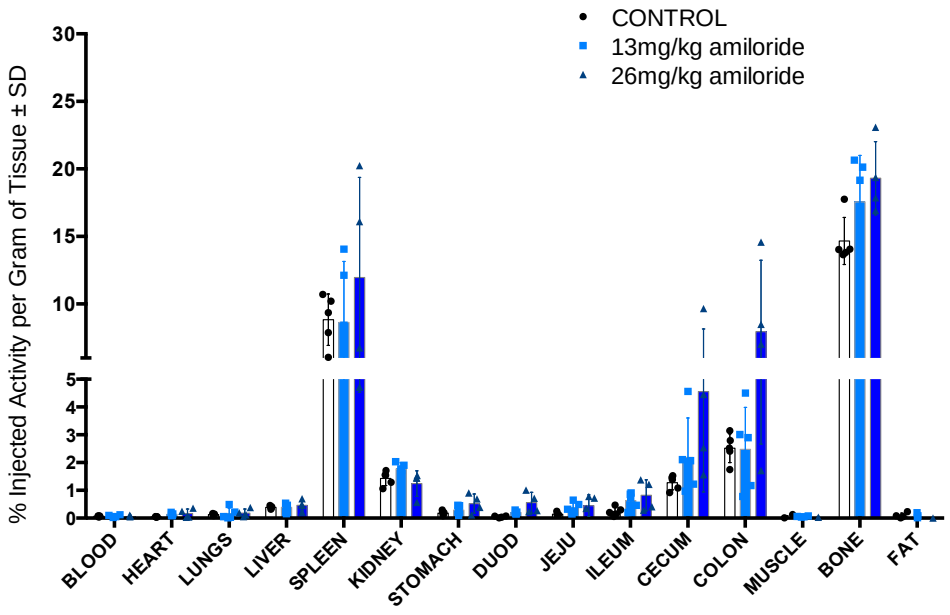

Supplemental Figure 2: Dosing optimization of amiloride comparing the radioactive organ distribution at 24 h p.i. with 13 mg/kg and 26 mg/kg administered intraperitoneally 1 h prior combination with [^{223}Ra]$RaCl_2$, administered intravenously.

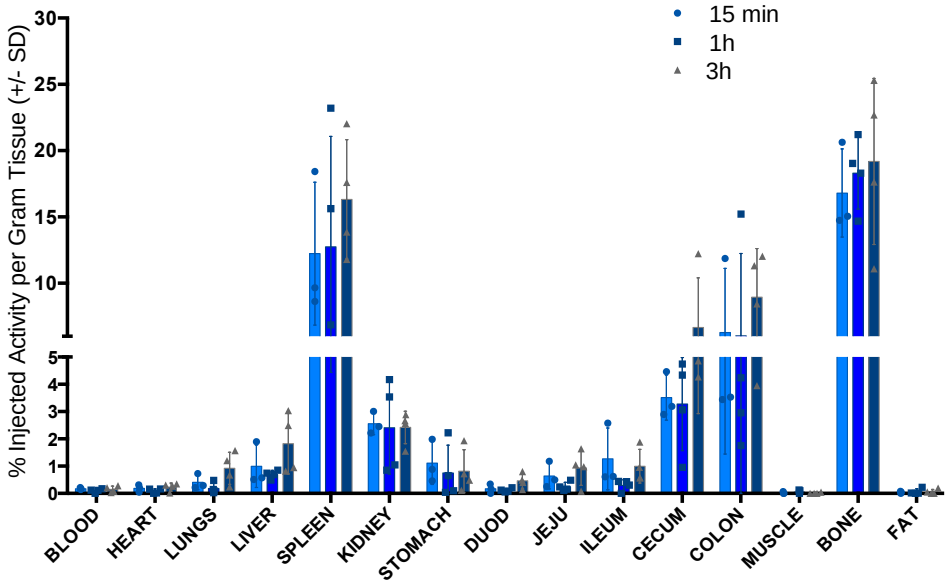

Supplemental Figure 3: Timing optimization of amiloride injection (intraperitoneal) at 13 mg/kg combined with [^{223}Ra]$RaCl_2$ (intravenously) conducted comparing whole organ distribution collected at 24 h post radioactive administration.

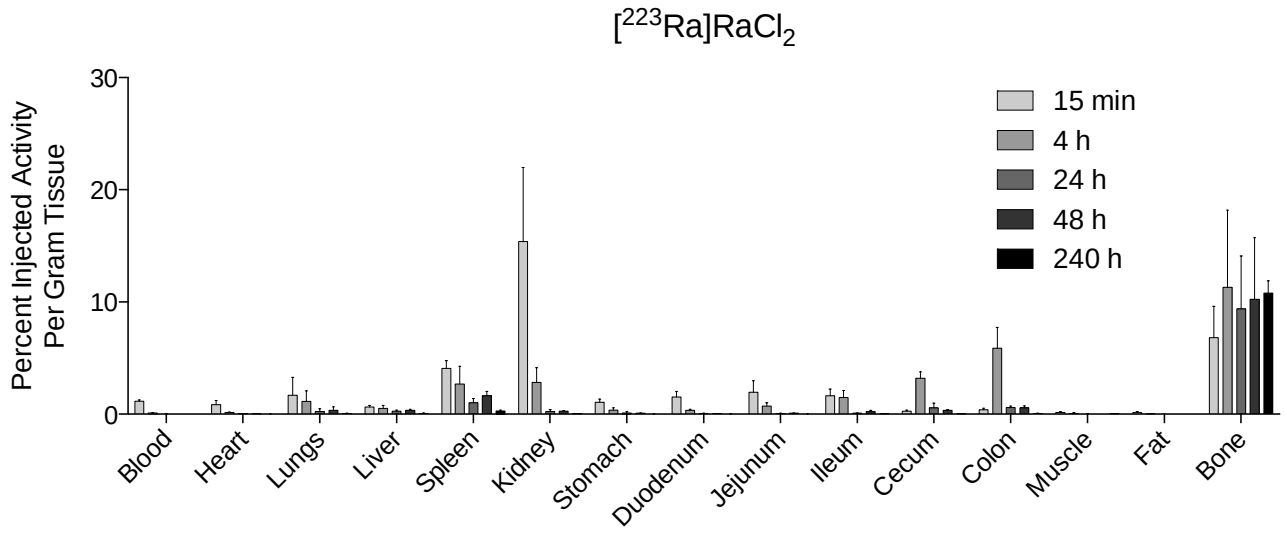

Supplemental Figure 4: [^{223}Ra]$RaCl_2$ organ distribution (%IA/g) in healthy skeletally mature mice Bl6/C57 (aged >10 weeks) from 15 min to 10 days

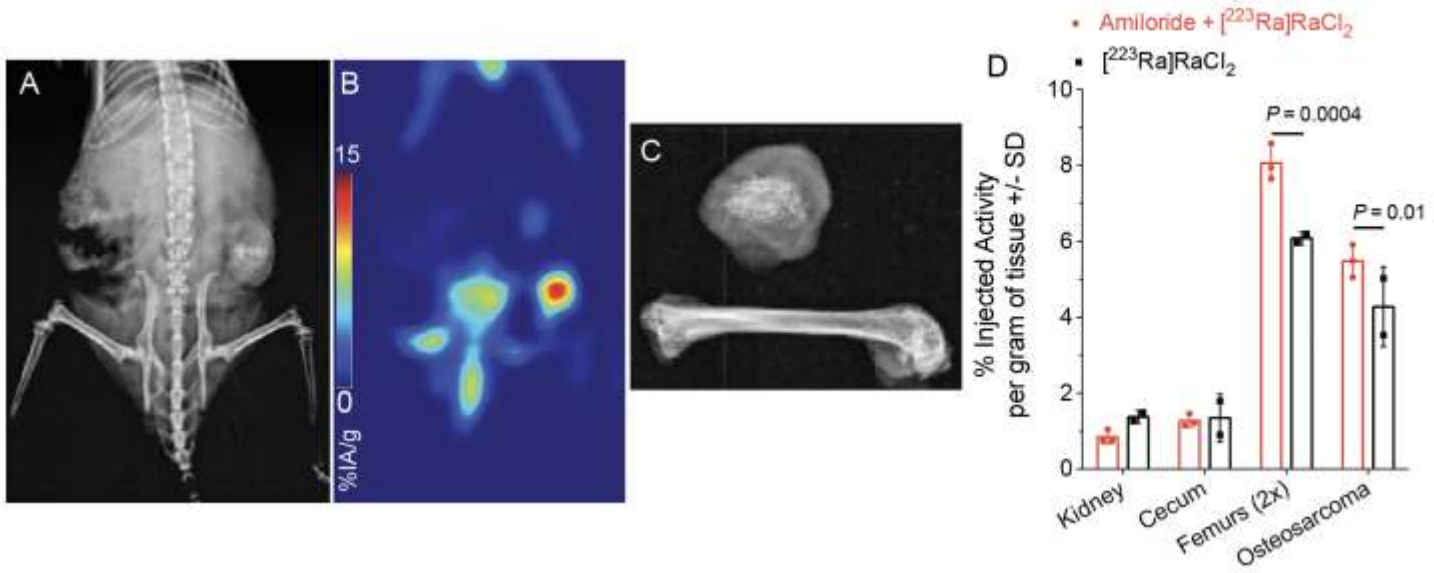

Supplemental Figure 5: Effect of amiloride on Radium-223 Uptake in Osteosarcoma Xenograft: A) Whole-body X-ray images of mice bearing flank SAOS2 xenografts; B) Whole-body [^{18}F]NaF PET scan of osseous tissue, at day of treatment. C) *Ex vivo* radiographs of extracted diseased mineral tissues and femur. D) Tissue uptake 24 h post-administration comparing combination amiloride to saline with [^{223}Ra]$RaCl_2$. No difference in renal or gut uptake was noted. Increased ^{223}Ra uptake in long bones and in the pathological osseous sites were observed for the combination ENaC treated group.

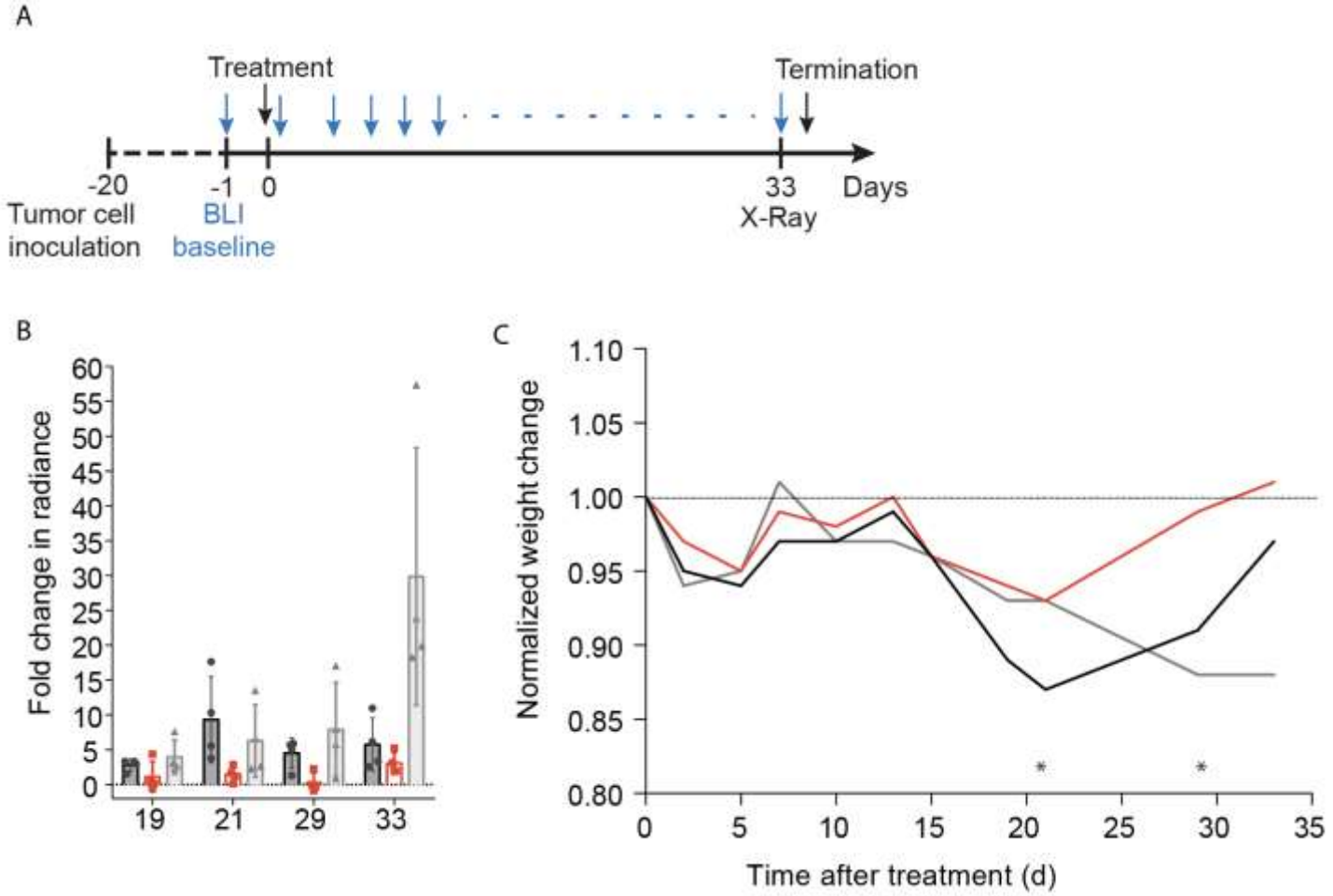

Supplemental Figure 6: A) Cells (C4-2B) were inoculated in the tibia shaft 20 days prior treatments. Animals were monitored over 35 days with indicated imaging and treatment from tumor inoculation to termination. B) Fold change of tumor radiance normalized to that of treatment day. C) Mice average normalized weight showing regain of weight for the combination cohort in contrast to the 2 other groups failing to return to initial weight. * indicates $P \leq 0.05$ at day 21 and 29 comparing [^{223}Ra]$RaCl_2$ with combination.

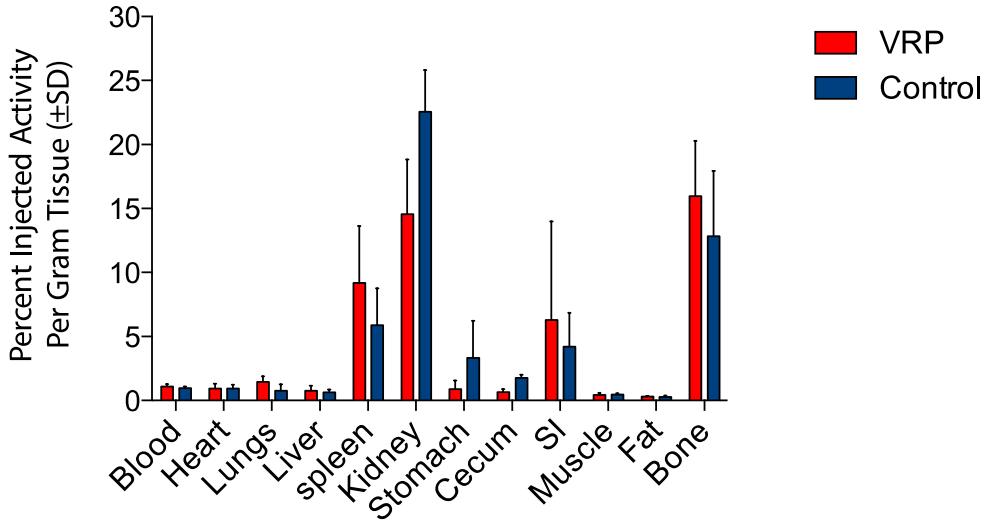

Supplemental Figure 7: ^{223}Ra organ distribution 1 h post [^{223}Ra]$RaCl_2$ administration, comparing the combination verapamil (VRP) (Ca^{2+} channel blocker) with [^{223}Ra]$RaCl_2$. Animals were administered VRP intraperitoneally 1 h prior radiopharmaceutical administration. None of the organs except the cecum presented any statistical differences considering *P* values (student's T test).

SUPPLEMENTAL TABLES:

	Saline + Radium-223			Amiloride + Radium-223			NS-1619 + Radium-223		
%IA	15 min (n=6)	1h (n=6)	4h (n=6)	15 min (n=6)	1h (n=6)	4h (n=6)	15 min (n=6)	1h (n=6)	4h (n=6)
Blood	0.66 ± 0.14	0.21 ± 0.04	0.07 ± 0.02	0.82 ± 0.12	0.23 ± 0.04	0.08 ± 0.02	0.72 ± 0.16	0.22 ± 0.05	0.07 ± 0.02
Heart	0.30 ± 0.09	0.13 ± 0.03	0.05 ± 0.02	0.38 ± 0.07	0.12 ± 0.02	0.05 ± 0.03	0.42 ± 0.08	0.11 ± 0.02	0.04 ± 0.02
Lungs	0.31 ± 0.16	0.21 ± 0.09	0.09 ± 0.04	0.33 ± 0.09	0.23 ± 0.11	0.12 ± 0.05	0.47 ± 0.19	0.22 ± 0.10	0.07 ± 0.02
Liver	1.01 ± 0.55	0.51 ± 0.30	0.12 ± 0.06	1.07 ± 0.59	0.42 ± 0.20	0.13 ± 0.06	1.01 ± 0.42	0.52 ± 0.14	0.10 ± 0.05
Spleen	0.28 ± 0.06	0.73 ± 0.32	0.36 ± 0.25	0.40 ± 0.15	0.56 ± 0.21	0.35 ± 0.12	0.72 ± 0.25	0.57 ± 0.17	0.37 ± 0.14
Kidney	6.66 ± 3.29	2.39 ± 0.79	0.37 ± 0.10	3.64 ± 1.72	2.40 ± 1.05	0.63 ± 0.21	6.21 ± 3.04	2.20 ± 1.15	0.46 ± 0.21
Stomach	0.94 ± 0.47	0.44 ± 0.22	0.27 ± 0.20	0.78 ± 0.40	0.38 ± 0.08	0.22 ± 0.14	1.33 ± 0.21	0.83 ± 0.39	0.26 ± 0.10
Duodenum	0.68 ± 0.39	0.18 ± 0.06	0.05 ± 0.04	0.45 ± 0.07	0.21 ± 0.10	0.08 ± 0.07	0.50 ± 0.29	0.26 ± 0.08	0.09 ± 0.09
Ileum	0.58 ± 0.38	0.95 ± 1.02	0.12 ± 0.09	0.51 ± 0.29	1.75 ± 1.29	0.19 ± 0.26	0.78 ± 0.40	1.52 ± 0.60	0.21 ± 0.21
Jejunum	0.33 ± 0.18	0.34 ± 0.28	0.24 ± 0.16	0.31 ± 0.12	0.57 ± 0.55	0.17 ± 0.17	0.26 ± 0.12	0.42 ± 0.31	0.18 ± 0.08
Cecum	0.23 ± 0.17	0.77 ± 0.35	1.52 ± 0.48	0.19 ± 0.03	1.01 ± 0.54	2.67 ± 1.17	0.27 ± 0.10	0.70 ± 0.50	2.01 ± 1.22
Colon	0.17 ± 0.05	0.20 ± 0.09	1.96 ± 0.83	0.19 ± 0.03	0.20 ± 0.06	1.45 ± 0.80	0.18 ± 0.02	0.17 ± 0.04	2.33 ± 0.65
Muscle	0.05 ± 0.03	0.04 ± 0.01	0.01 ± 0.01	0.05 ± 0.02	0.03 ± 0.02	0.02 ± 0.01	0.06 ± 0.02	0.05 ± 0.04	0.00 ± 0.01
Fat	0.05 ± 0.03	0.01 ± 0.01	0.00 ± 0.00	0.04 ± 0.04	0.01 ± 0.01	0.01 ± 0.01	0.03 ± 0.02	0.02 ± 0.01	0.00 ± 0.00
Bone	0.59 ± 0.17	0.69 ± 0.30	1.19 ± 0.24	0.59 ± 0.29	0.88 ± 0.35	1.83 ± 0.30	0.33 ± 0.11	0.67 ± 0.14	1.17 ± 0.16

	Saline + Radium-223			Amiloride + Radium-223			NS-1619 + Radium-223		
%IA/g	15 min (n=6)	1h (n=6)	4h (n=6)	15 min (n=6)	1h (n=6)	4h (n=6)	15 min (n=6)	1h (n=6)	4h (n=6)
Blood	2.17 ± 0.19	0.65 ± 0.08	0.20 ± 0.03	2.47 ± 0.27	0.77 ± 0.13	0.26 ± 0.03	2.08 ± 0.30	0.65 ± 0.12	0.18 ± 0.04
Heart	1.56 ± 0.50	0.56 ± 0.27	0.24 ± 0.10	2.12 ± 0.34	0.66 ± 0.10	0.27 ± 0.10	2.04 ± 0.39	0.60 ± 0.08	0.20 ± 0.08
Lungs	1.44 ± 0.66	1.03 ± 0.52	0.42 ± 0.19	1.57 ± 0.45	0.96 ± 0.39	0.53 ± 0.23	2.21 ± 0.76	1.07 ± 0.41	0.35 ± 0.11
Liver	1.15 ± 0.74	0.52 ± 0.33	0.14 ± 0.06	1.29 ± 0.71	0.46 ± 0.21	0.16 ± 0.07	1.30 ± 0.74	0.66 ± 0.19	0.11 ± 0.06
Spleen	3.24 ± 1.02	8.51 ± 2.80	4.85 ± 2.92	6.19 ± 2.34	8.16 ± 3.91	4.81 ± 1.52	9.38 ± 3.20	8.04 ± 1.85	4.77 ± 1.75
Kidney	36.68 ± 18.28	13.01 ± 4.09	2.17 ± 0.55	22.92 ± 10.99	14.22 ± 6.94	3.50 ± 0.95	35.70 ± 17.07	13.11 ± 7.44	2.87 ± 1.34
Stomach	1.39 ± 0.60	0.76 ± 0.47	0.44 ± 0.37	1.28 ± 0.72	0.67 ± 0.23	0.40 ± 0.25	2.73 ± 0.44	1.32 ± 0.55	0.40 ± 0.15
Duodenum	3.27 ± 1.62	0.96 ± 0.24	0.32 ± 0.23	2.61 ± 0.26	1.24 ± 0.50	0.51 ± 0.37	2.69 ± 1.51	1.34 ± 0.42	0.51 ± 0.45
Ileum	3.27 ± 1.25	5.30 ± 5.17	1.08 ± 0.61	3.59 ± 1.91	10.43 ± 6.37	1.18 ± 1.29	4.47 ± 1.81	8.41 ± 3.19	1.20 ± 1.09
Jejunum	2.33 ± 1.35	2.86 ± 2.11	1.83 ± 1.09	2.24 ± 0.80	5.25 ± 4.74	1.61 ± 1.41	1.88 ± 0.81	3.27 ± 2.26	1.48 ± 0.57
Cecum	0.43 ± 0.27	1.35 ± 0.65	3.02 ± 1.12	0.37 ± 0.04	2.32 ± 1.37	6.28 ± 3.73	0.50 ± 0.19	1.39 ± 0.88	3.77 ± 2.10
Colon	0.97 ± 0.31	1.17 ± 0.56	8.91 ± 4.16	1.18 ± 0.36	1.07 ± 0.32	6.49 ± 3.28	1.13 ± 0.48	0.96 ± 0.27	9.62 ± 2.62
Muscle	0.41 ± 0.18	0.25 ± 0.01	0.06 ± 0.06	0.37 ± 0.12	0.28 ± 0.14	0.14 ± 0.07	0.46 ± 0.13	0.41 ± 0.38	0.03 ± 0.08
Fat	0.36 ± 0.22	0.12 ± 0.14	0.04 ± 0.03	0.26 ± 0.16	0.09 ± 0.04	0.05 ± 0.09	0.25 ± 0.12	0.11 ± 0.08	0.01 ± 0.02
Bone	6.83 ± 3.35	9.60 ± 4.80	13.96 ± 4.32	7.45 ± 2.31	13.60 ± 7.29	22.62 ± 3.24	3.80 ± 0.62	9.41 ± 2.48	15.79 ± 2.84

Supplemental Table 1: Numerical values % Injected Activity (IA) and % IA/gram (n=6) and statistics using the student t-test P values of ^{223}Ra whole organ distribution presented in Figure 2A comparing [^{223}Ra]$RaCl_2$; with Amiloride + [^{223}Ra]$RaCl_2$ and NS-1619 + [^{223}Ra]$RaCl_2$ at 15 min, 1 h and 4 h post [^{223}Ra]$RaCl_2$ administration

	15 min			4 h			24 h			48 h			240 h		
Combination	Mean (%IA/g)	SD	n	Mean (%IA/g)	SD	n	Mean (%IA/g)	SD	n	Mean (%IA/g)	SD	n	Mean (%IA/g)	SD	n
Blood	1.286136	0.1680353	4	0.1263299	0.02707957	4	0.02791498	0.00706568	4	0.007460109	0.00412874	4	0.02205042	0.00980587	4
Heart	1.157887	0.2626306	4	0.1136984	0.01952666	4	0.0451764	0.0302837	4	0.0387573	0.01660495	4	0.02262329	0.01746565	4
Lungs	4.213633	2.863407	4	0.5598086	0.615557	4	0.4293593	0.5592576	4	0.1448156	0.1761845	4	0.2928722	0.2434169	4
Liver	1.174585	0.3116064	4	0.4847367	0.3016431	4	0.2809911	0.1473182	4	0.202307	0.1724876	4	0.1054092	0.08302517	4
Spleen	3.980962	1.649713	4	2.091122	0.7017254	4	1.076818	0.6191714	4	1.379065	0.2882899	4	0.7410591	0.1591555	4
Kidney	15.64385	7.404927	4	1.901285	0.8503923	4	0.3228253	0.1848896	4	0.2558807	0.05419715	4	0.08307688	0.01423772	4
Stomach	0.6877006	0.1149299	4	0.3753085	0.4441946	4	0.4243939	0.2457922	4	0.1675111	0.07751615	4	0.03871745	0.02140627	4
Duodenum	1.583079	0.6404865	4	0.3430845	0.04867064	4	0.09636526	0.03002037	4	0.04478013	0.02044326	4	0.03218402	0.02918036	4
Jejunum	1.886994	0.8238677	4	1.089947	0.444753	4	0.1811629	0.1052425	4	0.07035638	0.0280624	4	0.02390192	0.01156451	4
Ileum	1.100085	0.4817129	4	1.670939	1.23118	4	0.4504758	0.1035889	4	0.1660643	0.06758376	4	0.02209063	0.01136822	4
Cecum	0.2365118	0.05015518	4	3.305635	2.760669	4	0.7955292	0.3130657	4	0.2945002	0.1428603	4	0.0448446	0.01899982	4
Colon	0.7195342	0.1887262	4	4.506662	2.624808	4	1.106817	0.3928619	4	0.6158786	0.3374675	4	0.07782671	0.02325246	4
Muscle	0.2653613	0.1414104	4	0.05186733	0.0243437	4	0.0563924	0.06485684	4	0.06191725	0.0748892	4	0.07579432	0.04400966	4
Fat	0.09526733	0.04822477	4	0.02147359	0.0195352	4	0.007696052	0.00474124	4	0.001670262	0.01081174	4	0.05655225	0.02224042	4
Bone	4.097728	1.15579	4	8.885285	4.436336	4	16.74254	2.742961	4	16.67759	8.223642	4	10.56088	3.498785	4

	15 min			4 h			24 h			48 h			240 h		
[^{223}Ra]RaCl$_2$	Mean (%IA/g)	SD	n	Mean (%IA/g)	SD	n	Mean (%IA/g)	SD	n	Mean (%IA/g)	SD	n	Mean (%IA/g)	SD	n
Blood	1.169538	0.09391656	4	0.1175373	0.01401238	4	0.01734663	0.01077043	4	0.01505588	0.00464882	4	0.006340256	0.00406584	4
Heart	0.8432367	0.3732072	4	0.1532283	0.03274979	4	0.04057152	0.02742222	4	0.04119933	0.01166959	4	0.004382428	0.02268926	4
Lungs	1.682146	1.603887	4	1.130225	0.9612913	4	0.2313552	0.2633644	4	0.3409219	0.3254534	4	0.0578289	0.02354648	4
Liver	0.6280642	0.1558409	4	0.5203158	0.2788523	4	0.2591377	0.09680536	4	0.3389141	0.09255996	4	0.06476675	0.05741169	4
Spleen	4.089929	0.6840701	4	2.69554	1.557598	4	1.022419	0.3719779	4	1.636318	0.4054865	4	0.2882278	0.07591362	4
Kidney	15.38772	6.590871	4	2.828296	1.3013	4	0.2426343	0.1712796	4	0.2571676	0.0669317	4	0.04087569	0.00774256	4
Stomach	1.05076	0.2781586	4	0.3717034	0.1899036	4	0.124045	0.09203762	4	0.08414359	0.02250614	4	0.02125757	0.01147008	4
Duodenum	1.542569	0.504703	4	0.3408047	0.1088364	4	0.05678289	0.02361137	4	0.05606991	0.01328332	4	0.01675255	0.02078001	4
Jejunum	1.971558	1.004884	4	0.7009393	0.3130281	4	0.05096411	0.03533968	4	0.07919758	0.04484299	4	0.02081099	0.01346771	4
Ileum	1.641311	0.606918	4	1.487142	0.618979	4	0.0956083	0.02512994	4	0.2067748	0.1281618	4	0.03235535	0.00867425	4
Cecum	0.2738736	0.08864974	4	3.213955	0.5493559	4	0.5723614	0.4190339	4	0.3357381	0.08162646	4	0.03556774	0.01519967	4
Colon	0.3963575	0.1525496	4	5.880912	1.86738	4	0.586316	0.1284722	4	0.56862	0.1622569	4	0.06540006	0.02410631	4
Muscle	0.1656154	0.07440572	4	0.0640504	0.0772082	4	0.008208609	0.04498434	4	0.004148945	0.01037712	4	0.02768566	0.0279186	4
Fat	0.1336298	0.1099008	4	0.03355403	0.02639345	4	-0.01560238	0.02921376	4	0.000824541	0.0160607	4	0.00505117	0.01669823	4
Bone	6.806796	2.809202	4	11.31279	6.884089	4	9.375665	4.733264	4	10.24459	5.484949	4	10.78348	1.114516	4

Supplemental Table 2: Mean % Injected Activity per gram (%IA/g) ± SD (Standard Deviation) values of ^{223}Ra organ distribution (n=4 / group) of amiloride combination versus [^{223}Ra]RaCl$_2$ administered mice acquired from 15 min to10 days (values plotted in Figure 3E and Fig. s3).

Absorbed Dose (Gy)	Heart	Lungs	Liver	Spleen	Kidneys	Stomach	Intestine	Skeleton
Combination	0.01	0.04	0.01	0.12	0.02	0.03	0.02	1.43
[^{223}Ra]RaCl$_2$	0.01	0.04	0.01	0.13	0.02	0.02	0.03	1.07

Supplemental Table 3: Comparative organ dosimetry of combination Amiloride / [^{223}Ra]RaCl$_2$ with [^{223}Ra]RaCl$_2$ over 10 days

Supplemental References:

1. Abou DS, Pickett J, Mattson JE, Thorek DLJ. A Radium-223 microgenerator from cyclotron-produced trace Actinium-227. *Appl Radiat Isot*. 2017;119:36-42.

2. Noel G, Baetz NW, Staab JF, et al. A primary human macrophage-enteroid co-culture model to investigate mucosal gut physiology and host-pathogen interactions. *Sci Rep*. 2017;7:45270.

3. Foulke-Abel J, In J, Yin J, et al. Human enteroids as a model of upper small intestinal ion transport physiology and pathophysiology. *Gastroenterology*. 2016;150:638-649.e8.

4. Foulke-Abel J, In J, Kovbasnjuk O, Zachos NC. Human intestinal enteroids: a new model to study human rotavirus infection, host restriction and pathophysiology. *Journal of*. 2015.

5. Schindelin J, Arganda-Carreras I, Frise E, et al. Fiji: an open-source platform for biological-image analysis. *Nat Methods*. 2012;9:676-682.

6. Edelstein AD, Tsuchida MA, Amodaj N, Pinkard H, Vale RD, Stuurman N. Advanced methods of microscope control using μManager software. *J Biol Methods*. 2014;1:10.

7. Bolch WE, Eckerman KF, Sgouros G, Thomas SR. MIRD Pamphlet No. 21: A Generalized Schema for Radiopharmaceutical Dosimetry—Standardization of Nomenclature. *J Nucl Med*. 2009;50:477-484.

8. Miloudi H, Locatelli M, Autret G, et al. Application of rodes software to experimental biokinetic data for dose assessment in mice and rats. *J Radiol Prot*. 2017;37:564-583.

9. Locatelli M, Miloudi H, Autret G, et al. RODES software for dose assessment of rats and mice contaminated with radionuclides. *J Radiol Prot*. 2017;37:214-229.

10. Dondossola E, Casarin S, Paindelli C, et al. Radium 223-mediated zonal cytotoxicity of prostate cancer in bone. *J Natl Cancer Inst*. January 2019.

11. Ningaraj NS, Rao M, Hashizume K, Asotra K, Black KL. Regulation of blood-brain tumor barrier permeability by calcium-activated potassium channels. *J Pharmacol Exp Ther*. 2002;301:838-851.

12. Vidt DG. Mechanism of action, pharmacokinetics, adverse effects, and therapeutic uses of amiloride hydrochloride, a new potassium-sparing diuretic. *Pharmacotherapy*. 1981;1:179-187.